Attribute expression of fault-controlled karst—Fort Worth Basin, TX

Jie Qi, Bo Zhang and Kurt J. Marfurt*
ConocoPhillips School of Geology and Geophysics, University of Oklahoma

The UNIVERSITY *of* OKLAHOMA
Mewbourne College of Earth and Energy
ConocoPhillips School of Geology and Geophysics
ConocoPhillips

1. Introduction:

The word 'karst' is a German word which denotes the area of modern Slovenia known as Kras and to the ancient Roman as Carso. The well drained limestone terrain and extensive system of natural caverns makes Kras an important wine producing area. The word karst is now to describe carbonate terrain that have undergone significant diagenetic alteration which give rise to enhanced joints, caves, and collapse features. Karsting features play many rolls in oil and gas reservoirs. The Ordovician carbonate-karst are the main oil and gas reservoir in the Tarim Basin, China where its depth can reach 6 to 7 km (Chen et al., 2010). In the Central Basin Platform of west Texas, karst, dissolution, and diagenesis can not only forms the vuggy porosity reservoir rock, but also the anhydrite-filled updip seal (Duo, 2011). In shale resource plays, such as the Barnett Shale unconformably lying upon the Ellenburger in many areas of the Fort Worth Basin, karst can form 'geohazards', such that wells that intersect collapse features and diagenetically altered faults and joints produce so much water from the underlying aquifer that they need to be abandoned. In the Barnett and Eagle Ford shales, such hazards are often fault controlled, and many interpreters call this 'a string of pearls' (Schuelke, 2011). In the Mississippi lime play of northern Oklahoma and southern Kansas where the average oil cutoff is 5%, the deeper Ordovician-age karsted Arbuckle (Ellenburger equivalent) formation provides the capacity to dispose of the 95% water (Elebiju et al., 2009).

2. Regional Geology:

The Fort Worth Basin is one of several basins that formed during the late Paleozoic Ouachita Orogeny, generated by convergence of Laurasia and Gondwana (Bruner and Smosna, 2011). The Mississippian age organic-rich Barnett Shale gas reservoir is a major resource play in the Fort Worth Basin. It is extended over 28,000 mi^2, with most production coming from a limited area where the shale is relatively thick and sandwiched between effective hydraulic fracture barriers. Conformably overlying the Barnett is the Marble Falls Formation, which consists of a lower member of interbedded dark limestone and gray-black shale. Underlying the Barnett Shale are the Ordovician Viola-Simpson Formations, which mainly consist of dense limestone and dolomitic limestone and the lower Ordovician Ellenburger Group which consists of porous dolomite and limestone.

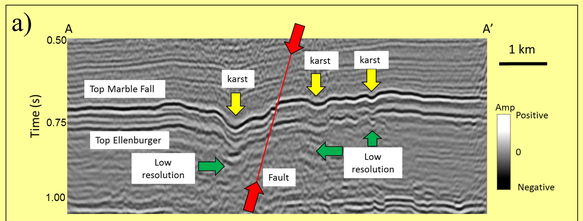

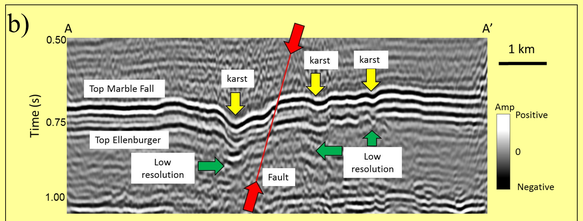

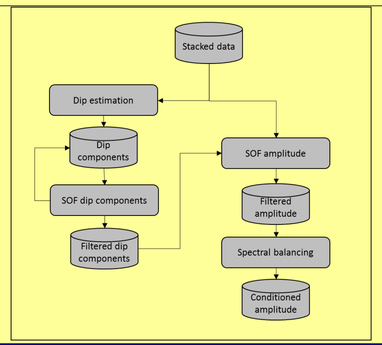

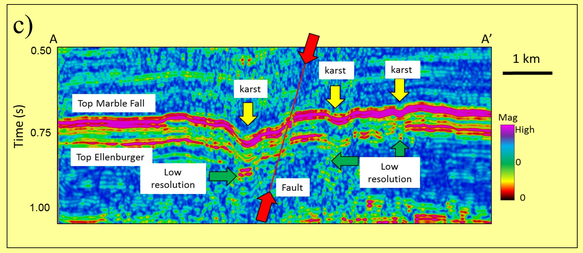

Figure 1. (a) Vertical slice along line AA' (a) before and (b) after application of the data conditioning workflow (an edge-preserving principal component structure-oriented filtering algorithm): dip estimate—SOF dip components—filtered dip components—SOF amplitude—filtered amplitude—spectral balancing—conditional amplitude. (c) is the 25 Hz spectral (a) vertical section.

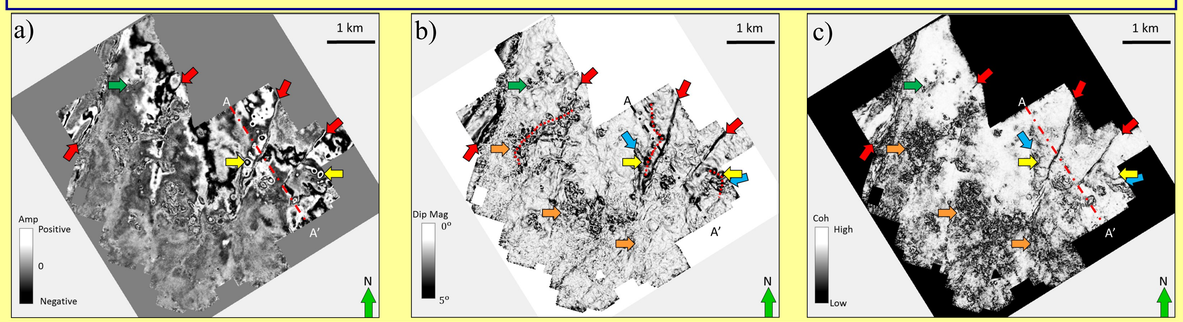

Figure 2. (a) Time slice at t=0.750 s through the seismic amplitude volume at the approximate top Ellenburger horizon. As seen in Figure 2b, the collapse features are delineated by steeply dipping edges which in this image appear as black ellipses. Red arrows indicate faults that control many of the larger collapse features. Dashed red lines show a "string of pearls" features which when correlated with most negative curvature indicates there control by diagenetically altered joints or faults with little vertical offset. We interpret the feature indicated by the blue arrows to be a valley or cave collapse. Green arrow indicates small scale karst that are far from major fault zones. (c) Time slice at t=0.750 s through eigenstructure-based coherence. Note that the faults (red arrows) and large collapse features (yellow arrows) do not appear as strong as in the dip magnitude image. Orange arrows indicate incoherent, rugose surfaces that are free of large collapse features.

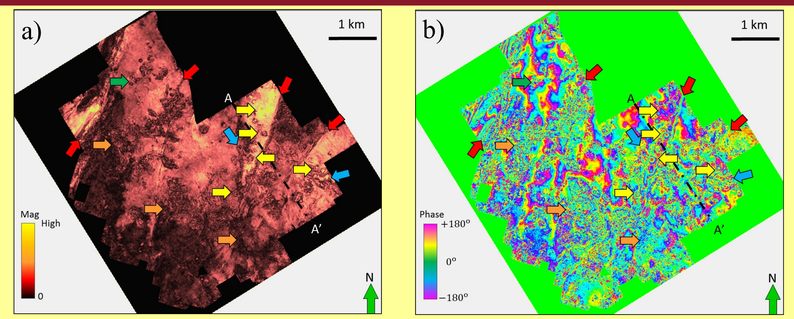

Figure 3. Time slice at t=0.750 s through (a) peak magnitude and (b) peak frequency phase component volumes. Red arrows indicate faults, blue arrows cave collapse and green arrow small karst shown on the previous image. Orange arrows indicate a relatively rugose surface that is free of large collapse features.

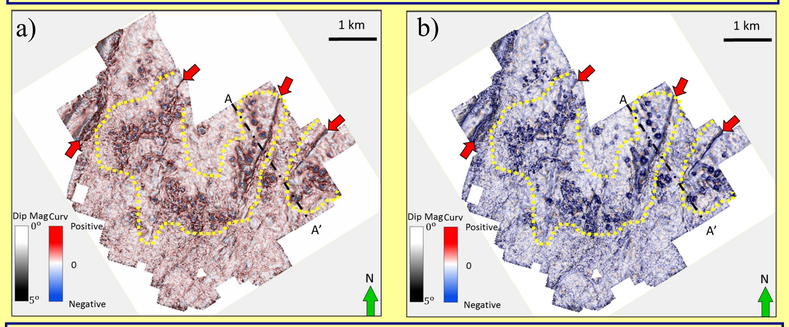

Figure 4. Time slices at t=0.750 s through (a) most-positive and (b) most-negative structural curvature co-rendered with dip magnitude. In this survey, the major faults are expressed by a positive curvature anomaly on the footwall which laterally offset from a corresponding a negative curvature anomaly on the hanging wall. The dip magnitude and coherence anomalies fall between the two curvature anomalies. In this image, the bowl shaped collapse features express a negative value and appear as blue ellipses (yellow and green arrows). The rugose surface (orange arrows) is represented by a shorter wavelength, lower deformation pattern. Yellow polygons indicate the area where large collapse features are controlled by faults.

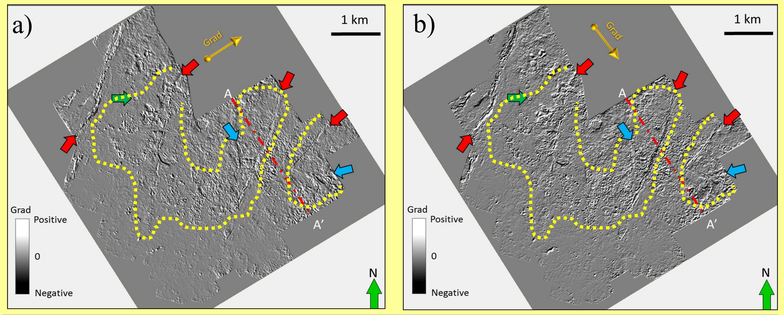

Figure 5. Time slices at t=0.750 s through (a) SW-NE and (b) NW-SE amplitude gradients computed along structural dip. Large karst do not appear to give a strong amplitude anomaly, although small karsts (green arrow) do. There does not appear to be significant acquisition footprint in either of the gradient images.

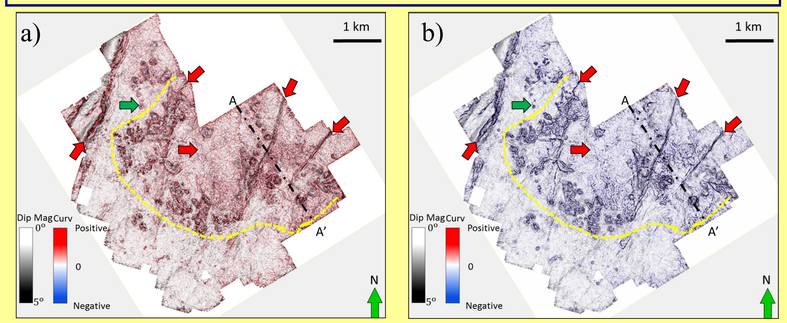

Figure 6. Time slices at t=0.750 s through (a) most-positive and (b) most-negative amplitude curvature volumes co-rendered with dip magnitude volumes. Dashed yellow polygons indicate areas of fault-controlled karsting. While structural curvature is computed by taking the derivative of the inline and crossline dip components, amplitude curvature is computed by taking the derivative of the inline and crossline amplitude gradients shown in the previous image. Yellow dashed line indicates zone dominated by fault controlled karst. Although NW-SE and NE-SW lineaments could be acquisition footprint, we interpret lineaments at other azimuths to indicate diagenetically altered joints giving rise to laterally variable reflectivity.

4. Conclusions:

Karst and fault play important roles under Barnett Shale and Ellenburger Group. The production of these reservoirs can be adversely impacted by karst features connected to the deeper aquifer. Interpreters will often ask, "Which attribute works best?" Our philosophy is to use multiple attributes that confirm a given geological hypothesis. Dissolution that gives rise to karst collapse will result in steeper dips surrouding negative curvature bowl-shaped anomalies. The chaotic infill will be seen as low coherence "fingerprints". Chaotic reflectivity will also result in destructive interference giving rise to a lower spectral frequency. Diagenetically altered joints and faults may be open, or cemented. In either case, they will give rise to lateral changes in amplitude measured by amplitude graidents and amplitude curvature. All of these architectural elements form part of a karst terrain including collapse features, karst towers, caves, joints, and rugose topography, that can be integrated using modern and paleo analogues to converge on a coherent interpretation.

5. Acknowledgements:
The authors would like to thank Marathon Oil for providing the data and key insight in the data analysis of this region. Financial support and most attribute computation was supported by the OU Attribute-Assisted Seismic Processing and Interpretation (Consortium). Data display was done using Petrel software provided to OU for use in research and education.

6. References:

Al-Dossary, S., and K. J. Marfurt, 2006, 3D volumetric multispectral estimates of reflector curvature and rotation: Geophysics, **71**, P41-P51.

Bahorich, M. S., and S. L. Farmer, 1995, 3D seismic discontinuity for faults and stratigraphic features: The coherence cube: 65th Annual International Meeting, SEG, Expanded Abstracts, 93-96.

Barnes, A. E., 2000, Weighted average seismic attributes: Geophysics, **65**, 275-285.

Bruner, K. R., and R. Smosna, 2011, A comparative study of the Mississippian Barnett Shale, Fort Worth basin, and Devonian Marcellus Shale, Appalachian basin: Technical Report DOE/NETL/2011/1478, National Energy Technology Laboratory for The United States Department of Energy.

Castagna, J. P., S. Sun, and R. W. Siegfried, 2003, Instantaneous spectral analysis: Detection of low-frequency shadows associated with hydrocarbons: The Leading Edge, **22**, 102-120.

Chopra, S., and K. J. Marfurt, 2013, Structural curvature versus amplitude curvature: The Leading Edge, **32**, 178-184.

Chopra, S. and K. J. Marfurt, 2010, Integration of coherence and curvature images: The Leading Edge, **29**, 1092-1107.

Donias, M., C. David, Y. Berthoumieu, O. Lavialle, S. Guillon, and N. Keskes, 2007, New fault attribute based on robust directional scheme: Geophysics, **72**, P39–P46.

Gale, J. F. W., R. M. Reed, and J. Holder, 2007, Natural fractures in the Barnett Shale and their importance for hydraulic fracture treatments: American Association Petroleum Geologists Bulletin, v 91, p. 603–622.

Gersztenkorn, A., and K. J. Marfurt, 1999, Eigenstructure-based coherence computations as an aid to 3D structural and stratigraphic mapping: Geophysics, **64**, 1468-1479.

Holtz, M. H., and C., Kerans, 1992, Characterization and categorization of West Texas Ellenburger reservoirs, in Candelaria, M. P., and Reed, C. L., eds., Paleokarst, karst related diagenesis and reservoir development: examples from Ordovician-Devonian age strata of West Texas and the Mid-Continent: Permian Basin Section SEPM Publication No. 92-33, 31–44.

For communication email Id: jie.qi@ou.edu